

Auger-driven Motion in Granular Media

Stephanie L. Chang and Paul B. Umbanhowar

December 10, 2017

Abstract

The purpose of this project was to create an underground locomotor capable of following user-defined, arbitrary trajectories. Numerous iterations of a modular robot mounted with an auger were fabricated. Rapid, empirical tests within a loosely packed bed of poppy seeds were performed to clarify how certain auger parameters influenced the robot's motion. A theoretical model was derived to describe how the parameters of an auger and granular material characteristics affect the amount of propulsive force generated. A final prototype was built and tested to verify the model. Suggestions for design improvements were posed based on results obtained from these experiments.

Contents

1	Introduction	1
2	Iteration Progression	2
3	Analytical Optimization	4
4	Optimized Augerbot Observations and Future Directions	8
5	Conclusion	9

1 Introduction

Subterranean navigation and operation is important for a sundry of tasks, such as mining, construction, reconnaissance and bomb detection. Although there are numerous robots available for working in water and hard earth, fewer options exist for exploring granular media environments. In the past, research into bio-inspired locomotion (legged (turtles) [6], undulating (snakes) [5] and push-me-pull-you (bivalves and protozoans) [7, 3, 1]) through sand has motivated the development of many mechanical systems. From extant technologies, helical motion is known to be an effective strategy for pulling bodies through solids (e.g drills) and fluids (e.g airplanes). However, little research has been conducted to examine the performance of helical motion in rheological matter. The burrowing robot project investigates how a rotating auger could be used to help robots “swim” within dry granular media. This study was largely influenced by two papers: “Helical Locomotion in a Granular Medium” and “A Terradynamics of Legged Locomotion on Granular Media” [2, 4].

In August 2017, Texier *et. al* developed a mathematical model that predicts the amount of propulsive force created by a wire coil (with a small fiber radius) moving horizontally through a tank of plastic beads. From experiments, the pulling force induced was found to depend linearly on the depth of the rotating helix. A method for computing optimal local inclination angles was verified for measured friction coefficient ratios. The relationship discovered between the helix’s translational speed and local inclination was subsequently used to validate our characterization of auger motion in granular media.

In [2], the coil movement was constrained to a horizontal track. Eventually, however, we want to build a robot capable of moving freely; as such, a model which considers arbitrary directions is required.

Li *et. al* employed finite element analysis to split the foot of a RHex robot into thin, rigid plates. When RHex scuttles across a granular substrate, the force and velocity vectors on each plate vary in direction, as does the angle. Vertical and horizontal stress per depth were measured for differently oriented tiles pushed through poppy seeds and 0.3 mm and 3 mm glass beads. Fourier transforms were subsequently applied to obtain generalized fitting approximations for normal and tangential friction coefficients sensitive to a plate's attack and intrusion angles. In this study, these equations as well as the zeroth- and first-order Fourier coefficients explicitly calculated for loosely-packed poppy seeds were used.

2 Iteration Progression

A robot with 5 main components was designed [Figure 1]. When powered, an Archimedes screw mounted at the head of the robot spun to part granular media and pull the robot forward. This was attached to an adapter plate which fit snugly around the shaft of a 12 V DC motor. A cylindrical cap on the motor itself stopped granules from falling into an exposed gear box. Wedged inside the protective cap were wings which would prevent the body of the robot from rotating with the screw. Lastly, an elongated hemispherical housing unit covered the back of the robot to shield soldered wire junctions from wear and tear. Note, a modular setup was created to make testing different combinations of screws and wing shapes easier.

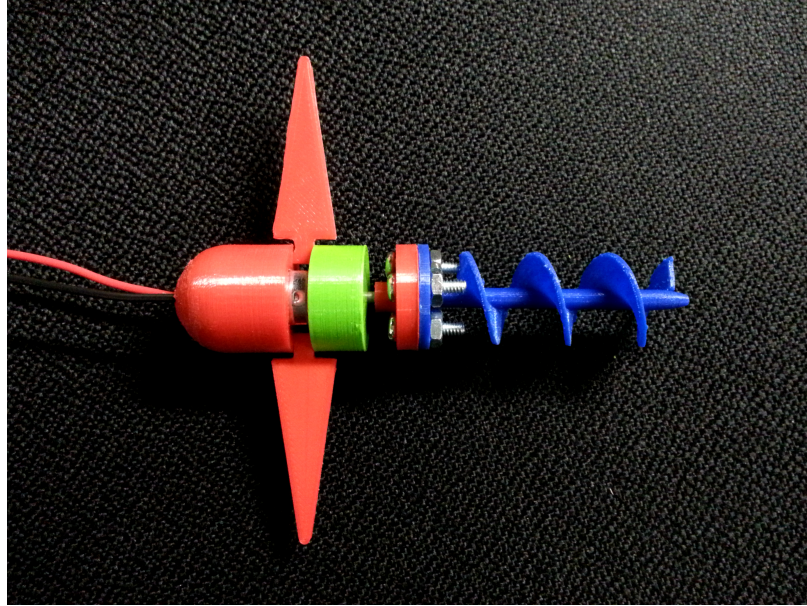


Figure 1: The first prototype of the augerbot

Multi-auger systems were rejected for this preliminary study to simplify the mechanics involved, mitigate human error during the assembly process, and accelerate the evolution of the robot's design. To test the prototypes, a 60" by 21" by 4" tank of poppy seeds with a volume fraction between 0.57 and 0.62 was used. Poppy seeds were chosen because the granules are roughly uniform in size.

For the first few iterations, all parts - aside from the motor and fasteners - were manufactured from PLA using an Ultimaker 3 3D Printer. To explore the parameter space, arbitrary dimensions were selected to create three augers and three pairs of wings [Figure 2]. The experiments listed in Table

1 were conducted for each prototype created. During the first round of testing, all auger and wing permutations for the components shown below were evaluated.

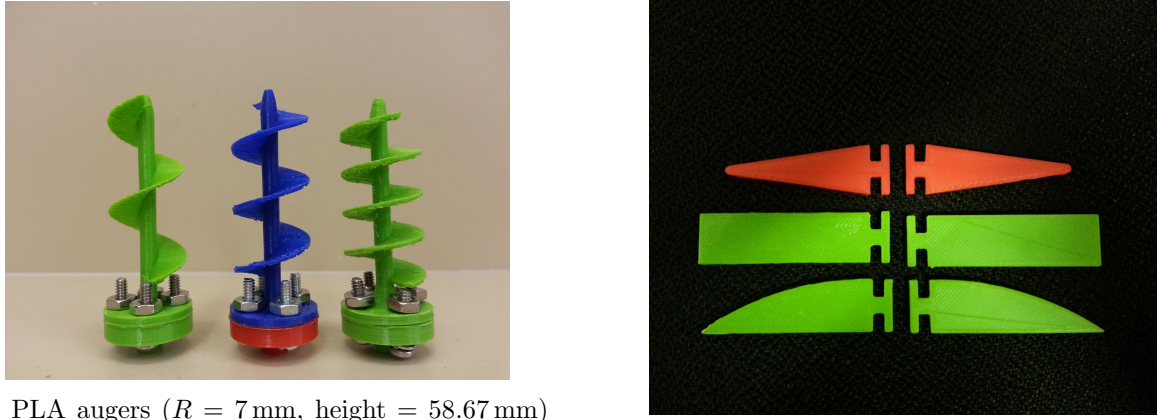


Figure 2: Trial 1 augers and wings

Table 1: Prototype tests

Test	Method
Submerged swimming	Robot starts inside the poppy seed bed with its wings parallel to the bottom of the tank
Surface swimming	Robot starts on top of the poppy seed bed with its wings parallel to the bottom of the tank
Burrowing	Robot starts at an angle with the auger nose pointed at the surface of the poppy seed bed

For both submerged and surface swimming, all auger and wing combinations failed: the prototypes simply rotated in place and, when buried, pitched upwards at varying rates. When the robot was introduced into the seeds at an angle, however, the 3-loop auger and curved wing pairing occasionally produced weak forward movement [Figure 3]. Some rotation was seen, possibly due to the influence of stiff, solid-core wires and the aft position of the center of mass. To increase the ratio of thrust to torque, a wider screw ($R = 20$ mm) with the same number of revolutions was designed. A captured nut fastening interface was integrated to streamline auger installation. The PLA helix adapter was also swapped out for a brass hub and set screw to move the center of mass between the wings and eliminate wobbling caused previously by frictional wear. With the new auger, no noticeable difference in performance was observed. However, when the robot was buried in the seeds, greater propulsive force was felt when the body was held prior to release.

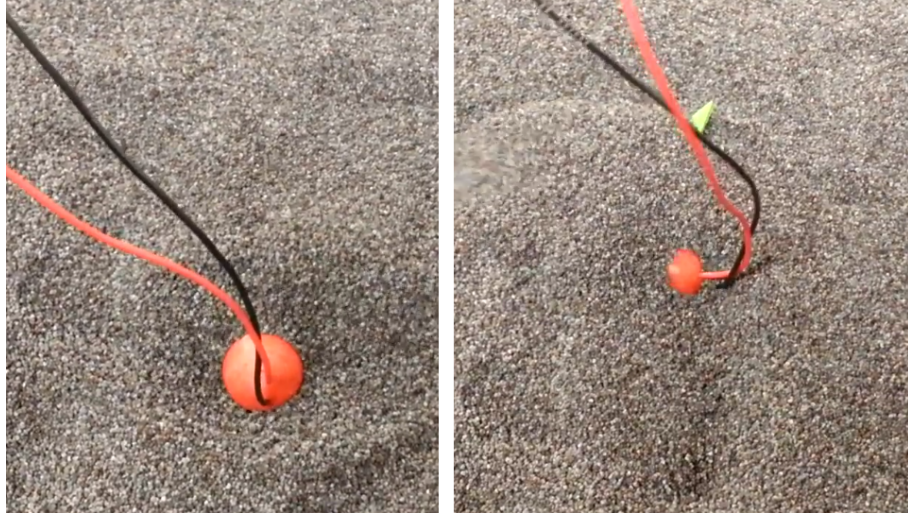


Figure 3: Forward translation observed for a prototype mounted with a 3-loop auger and curved wings

3 Analytical Optimization

To find the optimal parameters needed to maximize an auger's pulling ability, a more principled method - inspired by extant studies - was developed [2, 4].

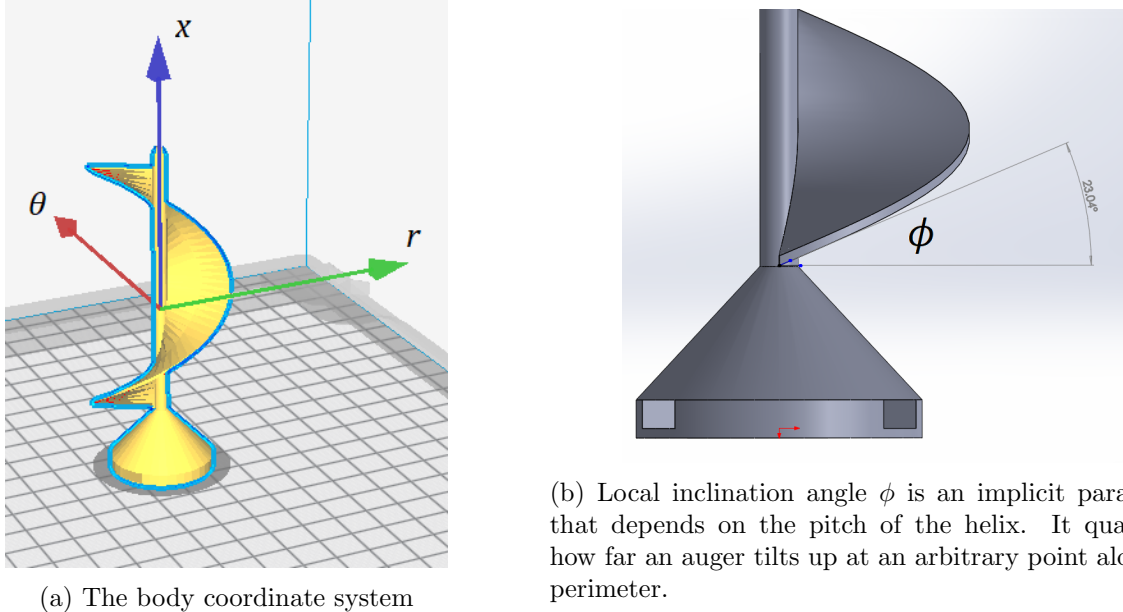


Figure 4: General problem set-up shown on an auger

A cylindrical coordinate system $(\vec{e}_r, \vec{e}_\theta, \vec{e}_x)$ was used to describe the helix [Figure 4a]. Local inclination angle ϕ , shown in Figure 4b, was used to define tangential unit vector $\vec{e}_t = \langle 0, \cos(\phi), \sin(\phi) \rangle$ and normal unit vector $\vec{e}_n = \langle 0, \sin(\phi), -\cos(\phi) \rangle$. For a tiny section along the helix path, the local velocity was determined to be $\vec{v} = \langle 0, rw, U \rangle$, where w represents the angular velocity about the auger's stem and U refers to the translational velocity along the x -axis. Note, the screw's radius and height were restricted to account for the dimensions of the poppy seed tank and the build volume of the Ultimaker 3.

Imagine an auger is composed of infinitesimal segments, each of which feels drag and thrust. According to resistive force theory, the amount of force generated by a body moving through granular media can be approximated by adding the forces experienced by each of its finite elements. $F_x(\phi, U)$, therefore, is the linear superposition of all local forces projected onto the x-axis. For an auger with radius R and n revolutions, this calculation looks like

$$F_x(\phi, U) = \int_0^R \int_0^{2\pi n} (\vec{f} \cdot \vec{e}_x) \frac{r}{\cos(\phi)} d\theta dr , \quad (1)$$

where \vec{f} denotes the force per unit area felt by each partition. Coulomb's law of friction was used to express \vec{f} as the sum of two force components tangential and normal to stem of the auger. Fleshed out, this equation takes the form

$$\begin{aligned} \vec{f} &= -C_t(\vec{e}_\nu \cdot \vec{e}_t)\vec{e}_t - C_n(\vec{e}_\nu \cdot \vec{e}_n)\vec{e}_n \\ &= \frac{-C_t(r\omega \cos(\phi) + U \sin(\phi))\vec{e}_t - C_n(r\omega \sin(\phi) - U \cos(\phi))\vec{e}_n}{\sqrt{U^2 + (r\omega)^2}} , \end{aligned} \quad (2)$$

where C_t and C_n represent depth- and ϕ - dependent tangential and normal stress coefficients respectively.

Plugging equation (2) into equation (1), the total amount of propulsive force generated by the auger in the x-direction was found to be

$$\begin{aligned} F_x(\phi, U) &= \frac{2\pi n}{\cos(\phi)} \left[(C_n - C_t)\omega \sin(\phi) \cos(\phi) \left(\frac{R}{2\omega^2} \sqrt{(R\omega)^2 + U^2} + \frac{U^2}{2\omega^3} \left(\ln \frac{U}{R\omega + \sqrt{(R\omega)^2 + U^2}} \right) \right) \right. \\ &\quad \left. - \frac{U}{\omega^2} (C_t \sin^2(\phi) + C_n \cos^2(\phi)) (\sqrt{(R\omega)^2 + U^2} - U) \right] \end{aligned} \quad (3)$$

where $\vec{e}_x = \langle 0, 0, 1 \rangle$. Introducing non-dimensional helix velocity $\tilde{U} = \frac{U}{R\omega}$, equation (3) was rearranged as follows

$$\begin{aligned} F_x(\phi, \tilde{U}) &= \frac{2\pi R^2 n}{\cos(\phi)} \left[\frac{1}{2} (C_n - C_t) \sin(\phi) \cos(\phi) \left[\sqrt{1 + \tilde{U}^2} + \tilde{U}^2 \ln \left(\frac{\tilde{U}}{1 + \sqrt{1 + \tilde{U}^2}} \right) \right] \right. \\ &\quad \left. - \tilde{U} (C_t \sin^2(\phi) + C_n \cos^2(\phi)) \left(\sqrt{1 + \tilde{U}^2} - \tilde{U} \right) \right] . \end{aligned} \quad (4)$$

When the system is at equilibrium, ϕ is the only parameter that controls the value of U . Recall, C_t and C_n both depend on ϕ . The steady-state case is important because, when thrust and drag are balanced, U is the constant velocity at which the auger advances along the x-direction. Algorithm 1, therefore, systematically varies $\phi \in (0, \frac{\pi}{2}]$ to find the ϕ_{opt} value which yields the highest U .

Algorithm 1 Helix Local Inclination Optimization

Knowns:

R, n, d, ω ▷ Auger radius, number of turns, auger depth, and angular velocity
 $0 < \varepsilon \ll 1$
 $F_x(\phi, U)$ ▷ Propulsive force generated in the horizontal direction

Compute: Maximum helix translational velocity U for different ϕ values

- 1: Calculate C_n and C_t ▷ Normal and tangential friction coefficients
 - 2: Let $\phi = 10 * \frac{\pi}{180}$
 - 3: **while** $\phi < 90 * \frac{\pi}{180}$ **do**
 - 4: $U_{guess} = \varepsilon$ ▷ Initialize the helix's x-direction velocity close to 0
 - 5: **while** $F_x(\phi, U_{guess}) > \varepsilon$ **do** ▷ Modified Newton-Raphson*
 - 6: $U_{guess} = U_{guess} - \frac{F_x(\phi, U_{guess})}{\frac{d}{dU} F_x(\phi, U_{guess})}$
 - 7: **end while**
 - 8: Store ϕ and U_{guess}
 - 9: $\phi = \phi + (1 * \frac{\pi}{180})$ ▷ Increment ϕ by 1 degree
 - 10: **end while**
 - 11: Find the ϕ which corresponds to the largest U_{guess} saved
-

*Omitting the absolute value operator ensures that Newton-Raphson will not be employed to solve for the U -intercept when the line tangent at U_{guess} crosses the U -axis at a value ≤ 0 . This is necessary because function $F_x(\phi, U)$ contains natural log terms.

If an auger is placed on its side, small segments along the body can be interpreted as tiny plates [Figure 5]. Regardless of its location around the x-axis, each segment has the same attack angle β . With this in mind, C_t and C_n were determined using fitting functions proposed by Li *et al.* For a prone helix translating axially within loosely packed poppy seeds ($\gamma = 0$), these force coefficients were computed using

$$C_t = [0.02 \sin(-2\beta) + 0.051 + 0.047 \cos(2\beta) + 0.053 \sin(2\beta)] d \quad (5)$$

and

$$C_n = [0.057 + 0.025 \sin(2\beta) - 0.026 \cos(2\beta)] d , \quad (6)$$

where d is a known depth.

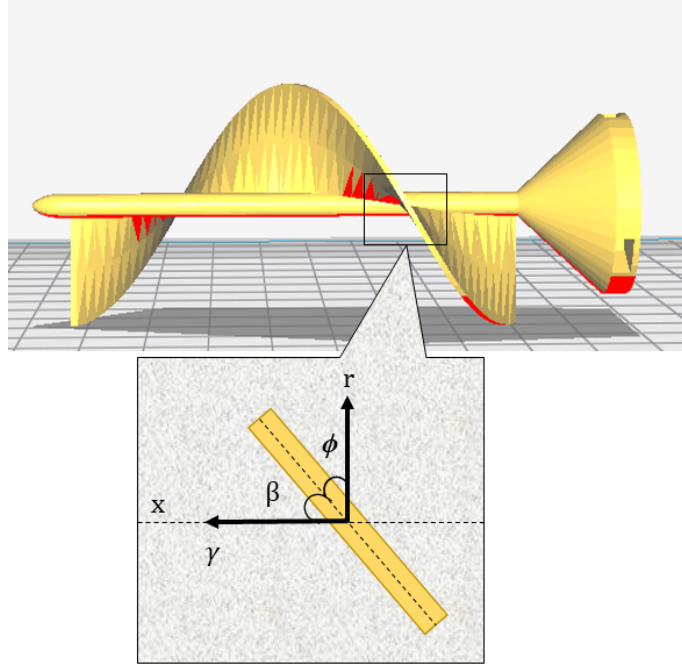


Figure 5: A plate element moving through granular media. Attack angle $\beta = \frac{\pi}{2} - \phi$ sets the tilt of the plate with respect to the horizontal plane. Intrusion angle γ defines the direction the plate moves with respect to the horizontal plane.

With explicit equations known for $F_x(\phi, U)$, C_t , and C_n , an aggressive auger was designed by first setting $R = 0.02$ m and $n = 1$. These values were arbitrarily chosen since R and n do not influence U when drag and thrust are balanced. Algorithm 1, using equations (3, 5-6), was then implemented to predict U for different values of ϕ [Figure 6]. Shown below, the maximum value of U (8.19736×10^{-2} m/s) occurs when $\phi = \phi_{opt} = 23^\circ$.

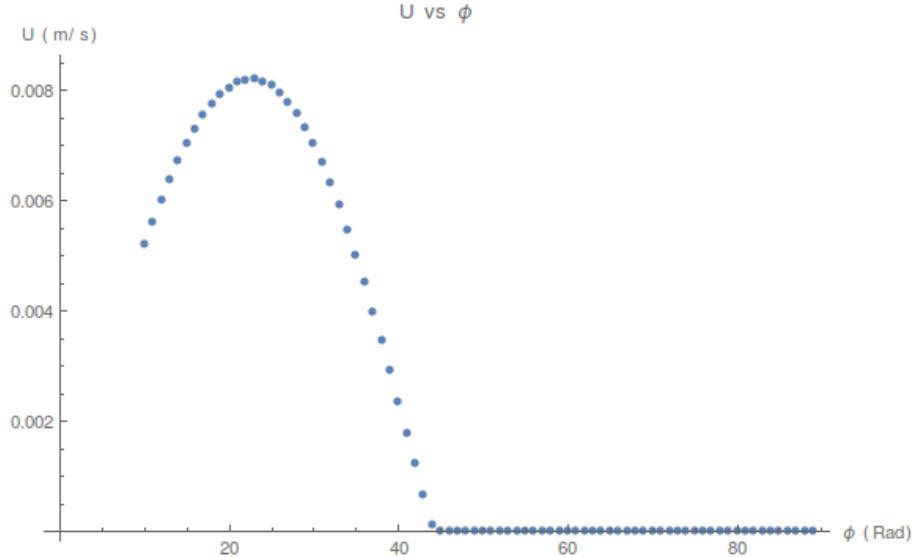


Figure 6: U (m/s) vs. ϕ (rad) for a prone auger ($R = 0.02$ m, $n = 1$, and $\omega = 3.51$ rad/s) moving in the x-direction buried at a depth of $d = 0.05$ m in loosely packed poppy seeds. ϕ was varied from 10° to 90° in increments of 1° .

4 Optimized Augerbot Observations and Future Directions

In SolidWorks, a new auger was modeled with dimensions corresponding to the optimal parameters found using algorithm 1 [Table 2]. Compared to the helices tested previously [Figure ??], the thickness of the profile swept along the path of the screw was increased to ensure the threads merged properly with the stem.

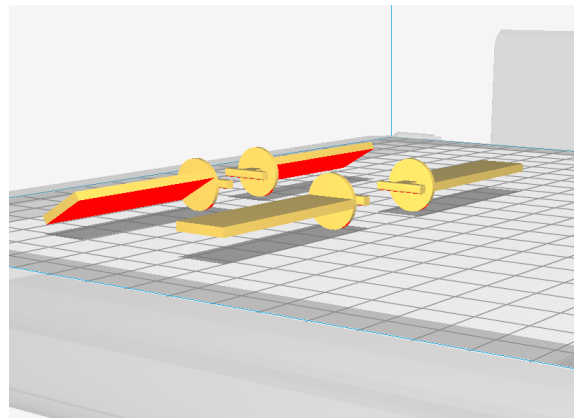
Table 2: Optimized Auger and Test Bed Parameters

Parameter	Value
Radius (R)	0.02 m
Revolutions (n)	1
Angular velocity (ω)	3.51 rad s ⁻¹
Depth (d)	0.05 m
Local inclination (ϕ_{opt})	23°
Sweep thickness	0.0025 m

Figure 7a shows the optimized auger prototype fastened onto the head of the robot. Like before, surface-skimming, diving and submerged experiments were run in a loosely packed bed of poppy seeds. The locomotive behaviors exhibited by the new robot were then compared against those observed for previous iterations. Wings parallel to the horizontal plane (0°) and wings tiled 30° with respect to the horizontal plane were also mixed and matched to adjust the trajectory of the robot.



(a) The optimized burrowing robot



(b) 40 mm x 12 mm wings oriented 0° and 30° with respect to the horizontal plane

Figure 7: Modular components used to tune the optimized robot

When the robot is buried horizontally 0.05 m underground, it does not advance forward. Instead, the stem tilts out of the poppy seed bed within a span of 2 seconds. Looking at the geometry of the auger, it is evident that a stress gradient, in the direction of gravity, contributes to the upward bias of the robot’s motion. To counter this resurfacing behavior, wings with a downward pitch could be added to ensure neutral buoyancy. Additional trim flaps could also be added to actively control the dive angle of the auger’s nose.

When the robot is placed horizontally on the surface of a freshly fluidized (i.e level) poppy seed bed, it spirals in the clockwise direction due to the right-handed asymmetry of the auger for all angles about the robot’s roll axis. This behavior matches that exhibited by previous prototypes. An attempt to produce counter-rotation using a 30° left wing and -30° right wing produced negligible results.

Larger wings or a rudder could be installed to neutralize the torque generated. A left-handed auger also be added adjacent to the existing right-handed auger.

When the robot penetrates the poppy seed bed at a sufficiently shallow angle with respect to the horizontal plane, some axial translation is observed [Figure 8]. Pointing the nose of the auger downwards prevents the robot from resurfacing immediately, giving it enough time to pull itself forward. This observation reinforces the need for further analysis into wing geometry and the development of actuated wing flaps.

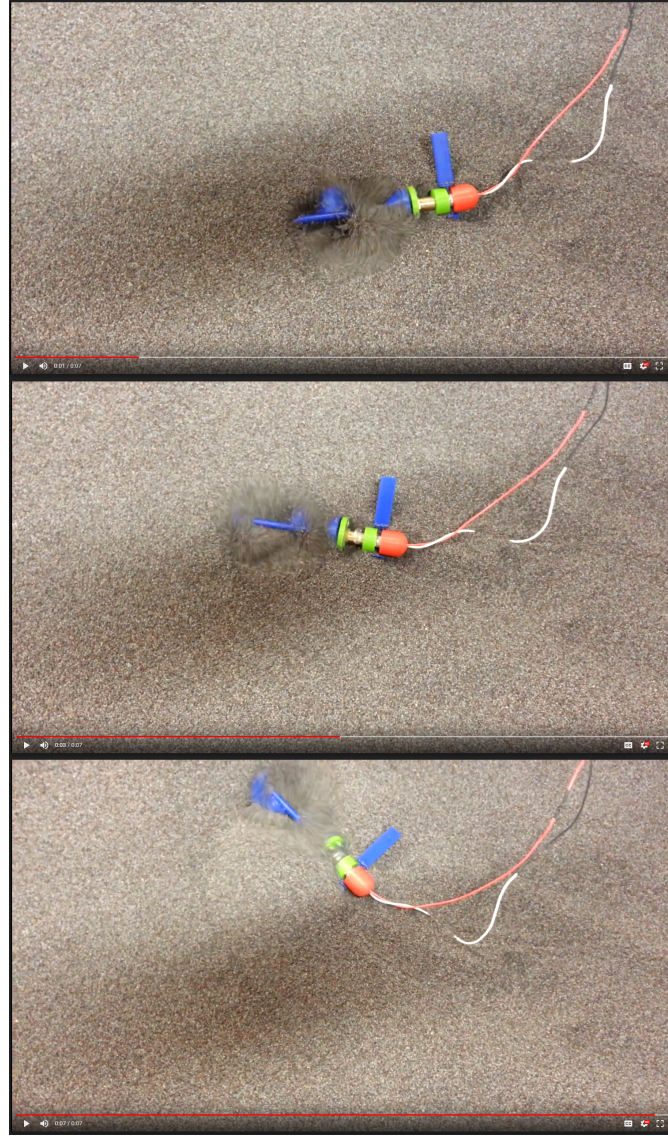


Figure 8: Successful forward progression with a $\phi_{opt} = 23^\circ$ auger

5 Conclusion

3D printing was used to rapidly produce numerous prototypes of a robot capable of moving freely within granular media. These iterations were tested in a loosely packed poppy seed bed to clarify the behavior of a prone, auger-bearing robot translating axially. To obtain a more informed view of the robot's mechanics, a theoretical model which optimizes the local inclination of an auger was

formulated. When a robot with the optimized screw was inserted into the seeds at a shallow angle, a significant improvement in forward movement was observed. For all iterations built, clockwise rotation due to yaw torque persisted. To restrict movement to the axial direction, further investigations into auxiliary accessories (e.g wings, rudders, trims) could be performed. Once mobility in 1-dimension is realized, motion planning and control for higher dimensional workspaces can be explored.

References

- [1] J E Avron, O Kenneth, and D H Oaknin. Pushmepullyou: an efficient micro-swimmer. *New Journal of Physics*, 7(1):234, 2005.
- [2] Baptiste Darbois Texier, Alejandro Ibarra, and F Melo. Helical locomotion in granular media. 119, 07 2017.
- [3] D P German and J P Carbajal. Burrowing behaviour of robotic bivalves with synthetic morphologies. *Bioinspiration & Biomimetics*, 8(4):046009, 2013.
- [4] Chen Li, Tingnan Zhang, and Daniel I. Goldman. A terradynamics of legged locomotion on granular media. *Science*, 339(6126):1408–1412, 2013.
- [5] Hamidreza Marvi, Chaohui Gong, Nick Gravish, Henry Astley, Matthew Travers, Ross L. Hatton, Joseph R. Mendelson, Howie Choset, David L. Hu, and Daniel I. Goldman. Sidewinding with minimal slip: Snake and robot ascent of sandy slopes. *Science*, 346(6206):224–229, 10 2014.
- [6] Nicole Mazouchova, Paul B Umbanhowar, and Daniel I Goldman. Flipper-driven terrestrial locomotion of a sea turtle-inspired robot. *Bioinspiration & Biomimetics*, 8(2):026007, 2013.
- [7] A G Winter, V, R L H Deits, D S Dorsch, A H Slocum, and A E Hosoi. Razor clam to roboclam: burrowing drag reduction mechanisms and their robotic adaptation. *Bioinspiration & Biomimetics*, 9(3):036009, 2014.